🔓 **Open Access**

High Strain Sensitivity Temperature Sensor Based on a Secondary Modulated Tapered Long Period Fiber Grating

Xiren Jin
Cuiting Sun
Shujie Duan
Weiliang Liu
Guoan Li
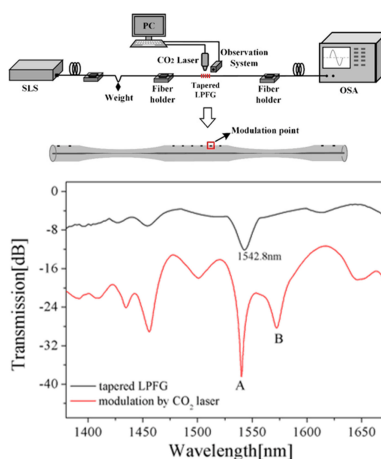Shuo Zhang
Xudong Chen
Lei Zhao
Chunlian Lu
Xinghua Yang
Tao Geng
Weimin Sun
Libo Yuan

High Strain Sensitivity Temperature Sensor Based on a Secondary Modulated Tapered Long Period Fiber Grating

Xiren Jin,[1] **Cuiting Sun** ⓘ**,**[1] **Shujie Duan,**[1] **Weiliang Liu,**[1] **Guoan Li,**[1]
Shuo Zhang ⓘ**,**[1] **Xudong Chen,**[1] **Lei Zhao,**[2] **Chunlian Lu,**[1]
Xinghua Yang,[1] **Tao Geng** ⓘ**,**[1] **Weimin Sun** ⓘ**,**[1] **and Libo Yuan** ⓘ [3]

[1]Key Lab of In-Fiber Integrated Optics, Ministry Education of China, Harbin Engineering University, Harbin 150001, China
[2]Aviation Key Laboratory of Science and Technology on Inertial Technology, FACRI, Xi'an 710065
[3]Photonics Research Center, Guilin University of Electronics Technology, Guilin 541004, China

Abstract: A novel sensor structure has been proposed and experimentally investigated for simultaneous strain and temperature measurement. The structure is fabricated by weak power modulation of CO_2 laser exposure on tapered long period fiber grating (LPFG). Compared with the transmission spectrum of the tapered LPFG, two peaks appear in the transmission spectrum of the novel structure. These resonance peaks exhibit different sensitivity responses; thus, simultaneous measurement of strain and temperature is realized by monitoring the wavelength shift of the two peaks. Experiment results indicate that strain sensitivities of the two peaks are 1.82 pm/$\mu\varepsilon$ and 8.17 pm/$\mu\varepsilon$, and temperature sensitivities are 47.9 pm/$^\circ$C and 65 pm/$^\circ$C, respectively.

Index Terms: Taper, CO_2 Laser, strain, temperature, simultaneous measurement.

1. Introduction

In recent decades, fiber grating devices have been investigated extensively owing to their excellent performance, such as small volume, low back reflection, wavelength domain response, resistance to electromagnetic interference, and sensitivity to multiple environmental parameters [1], [2]. However, cross-sensitivity problem in measurement can affect the performance of fiber grating devices. As simultaneous measurement is considered an effective way to solve the cross-sensitivity problem, it is of great importance in fiber grating devices. To address different requirements in various research fields, sensing characteristics have been selected for simultaneous measurement, such as simultaneous measurement of temperature and strain [3]–[5], temperature and refractive index (RI)
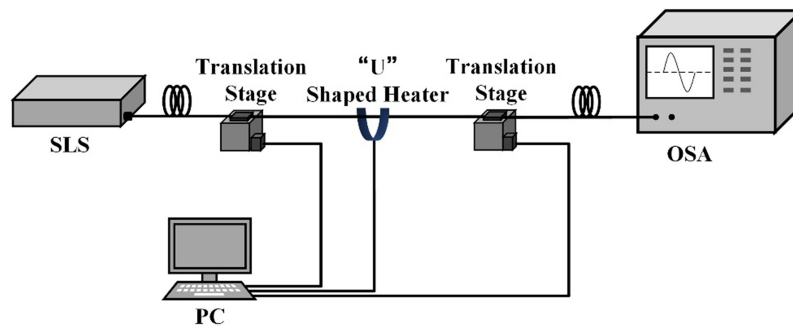
Fig. 1. Diagram of fabrication tapered long period fiber grating.

[6], temperature and torsion [7], temperature and magnetic field [8], liquid level and RI [9], shape and temperature [10], pressure and temperature [11], and others [12]–[14] Simultaneous measurement of strain and temperature is more widely used in some fields than other dual-parameter measurements, including automobiles, spacecraft, nondestructive evaluation of civil infrastructure, and environmental monitoring. Hence, several structures that can realize simultaneous measurement of strain and temperature have been proposed in recent years, including cascade long period fiber grating (LPFG) [15]; cascade fiber Bragg grating [16]; a fiber grating inscribed on a special optical fiber [17], [18]; an LPFG induced by electric-arc discharge [19]; an LPFG cascading another fiber structure, as combined with a tapered three-core fiber [20]; hybrid LPFG/MEFPI sensor [21]; micro-tapered fiber grating [22]; asymmetrical fiber Mach-Zehnder interferometer [23]; and others [24], [25]. It has been confirmed that these proposed structures can solve the problem of temperature interference during strain measurement, but they have a disadvantage of low strain sensitivity.

In this paper, a novel structure for simultaneous measurement of strain and temperature is proposed and validated through experiments. This structure is fabricated by weak power modulation of CO_2 laser exposure on a tapered LPFG. The proposed sensor has high strain sensitivity and is made of a normal single mode fiber with low material price. In addition, the proposed sensor has different mode interferences applicable to sensing applications for different parameters in future studies.

2. Fabrication and Principle

The tapered LPFG was fabricated using resistive filament heating; the experimental setup is illustrated in Fig. 1.

The tapering method was composed of two simultaneous process, heating process and elongation process. The single mode optical fiber (SMF28) was positioned at the center of the "U"-shaped resistive filament heater. The two ends of the fiber were mounted on the linear translation stages. The resistive filament heater heated the fiber and quickly softened it in the center of the 'U'-shaped heater. The filament's axial position was controlled by a stepper motor to make the two linear translation stages move in opposite directions during the heating process. Tension was applied to the softened fiber to produce a taper. After the first taper was produced, the optical fiber was shifted to a new position to produce the same taper. The above steps were repeated to produce five tapers in all. In our experiment, the pilling speed of the linear translation stage was about 1.2 mm/sec and heating temperature was maintained to be 1200 °C. The total length of a tapered region and its adjacent flat part is defined as period (Λ) of the tapered LPFG [26].

The schematic diagram of the tapered LPFG is displayed in Fig. 2. The length of each taper was 2.3 mm, the diameter of the taper was 62.5 μm, and the flat part between every two tapers was 2.5 mm. The period Λ of this grating was 4.8 mm.

Next, the tapered LPFG was modulated by weak power using the CO_2 laser. In this experiment, the accuracy of exposure time and modulated power was controlled by a self-developed program,
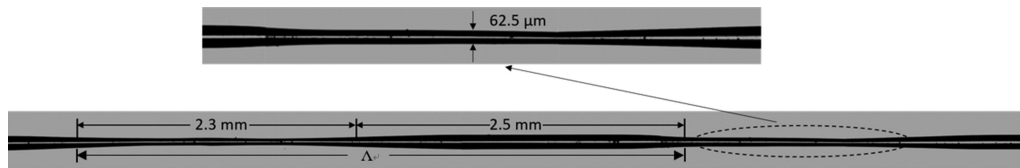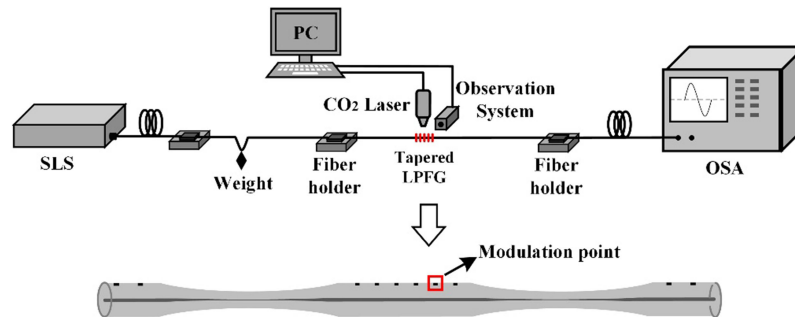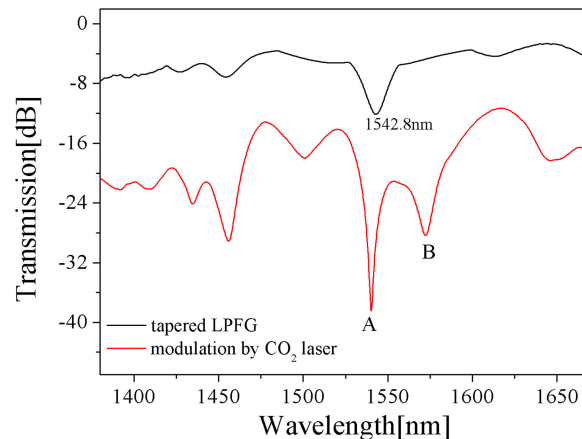
Fig. 2. Schematic diagram of tapered LPFG.

Fig. 3. The modulation device and schematic diagram of power modulation using CO_2 laser.

Fig. 4. Transmission spectrum of tapered LPFG and modulation after CO_2 laser.

the exposure time was set much less than the usual exposure time. There was no change in the geometry of the cladding. It was mainly the change in the refractive index at the modulation point. Therefore, it was a weak modulation process. The modulated regions are denoted by the flat sections between every two tapers. Each individual modulation region was radiated at six points by the laser. The distance between the two adjacent points was 500 μm within the individual modulation region. We scanned these modulated regions 10 to 12 times. An observation system was used for precise positioning during the laser radiation process. The modulation device and the schematic diagram of power modulation are shown in Fig. 3.

A Super-continuum Light Source (SLS) with a spectrum range of 600–1700 nm and an Optical Spectrum Analyzer (OSA) were connected to both ends of the fiber to monitor the transmission spectrum. In Fig. 4, the black curve depicts the transmission spectrum of the tapered LPFG; the red curve represents the transmission spectrum after modulation. Through weak modulation using a CO_2 laser, two peaks A and B appear in the modulation transmission spectrum compared with the original spectrum. Peak A was at 1540.2 nm, and Peak B was at 1572.2 nm.

Conventional coupled-mode theory is applicable to weak coupling under undisturbed optical fiber modes and the perturbation varies slowly along the fiber. A change in the refractive index

is considered an infinitesimal disturbance in the refractive index modulation of LPFG, and the field distribution of the optical fiber mode did not change in the modulation area. Therefore, the conventional coupled-model theory was used to analyze the refractive index modulation of LPFG in which the index perturbation is weak and occurs mainly in the core.

In terms of the structural modulation, the cladding region of the optical fiber was periodically tapered, and the effective refractive index in tapered and untapered regions could be modified periodically. The mode field distribution and refractive index distribution demonstrated clear changes in the modulation area, which could not be regarded as infinitesimal disturbance; it would elicit an error when analyzed using conventional coupled-model theory. However, the perturbation of the mode field can be regarded slow-varying but strong perturbation. The modal characteristics of waveguide were analyzed by using local coupled-mode theory [27], [28].

Considering the coupling of the fundamental mode and the co-directional cladding mode of LPFG, the coupling equation between the fundamental mode and the cladding modes can be expressed as follows

$$\begin{cases} \frac{da_{co}}{dz} = C(z) \cdot a_{cl} \exp\left\{i \int_0^z [\beta_{cl}(z) - \beta_{co}(z)]\, dz\right\} \\ \frac{da_{cl}}{dz} = -C(z) \cdot a_{co} \exp\left\{i \int_0^z [\beta_{co}(z) - \beta_{cl}(z)]\, dz\right\} \end{cases} \tag{1}$$

where a_{co} and a_{cl} denote the core mode field intensity and cladding mode field intensity, respectively; $C(z)$ is the coupling coefficient; $\beta_{co}(z)$ and $\beta_{cl}(z)$ represent the core mode propagation constant and cladding mode propagation constant, respectively; $C(z)$, $\beta_{co}(z)$, and $\beta_{cl}(z)$ are periodic functions related to the longitudinal z of the fiber, and the period is grating period Λ. Taking the Fourier expansion, $C(z)$ is expressed by

$$C(z) = \sum_{N=0}^{\infty} f_N \cdot \exp\left(i\frac{2N\pi}{\Lambda} z\right) \tag{2}$$

where f_N represents each harmonic coefficient after Fourier expansion, and N represents each harmonic component. By substituting Equation (2) into Equation (1), the phase detuning can be expressed as

$$\Delta\varphi = \int_0^z \left[\beta_{cl}(z) - \beta_{co}(z) + \frac{2N\pi}{\Lambda}\right] dz \tag{3}$$

Similar to traditional coupling mode theory, resonant coupling occurs when the phase matching condition is satisfied. As the propagation constant is periodic, phase matching should also be satisfied within a period at any random starting point z_0, such that $\Delta\varphi = \varphi(z_0 + \Lambda) - \varphi(z_0) = 0$. $\beta = 2\pi n_{eff}/\lambda$, n_{eff} is the effective refractive index. Phase matching conditions of LPFG can be expressed as

$$N\lambda = \int_{z_0}^{z_0+\Lambda} \left[n_{eff,co}(z) - n_{eff,cl}(z)\right] dz \tag{4}$$

where $n_{eff,co}(z)$ and $n_{eff,cl}(z)$ denote the effective refractive index of the core mode and cladding mode, respectively. The phase matching conditions in Equation (4) also apply to the tapered LPFG.

The Λ of the tapered LPFG was 4.8 mm, depicting an ultra-long-period fiber grating (ULPFG). In general, the ULPFG transmission spectrum demonstrates multiple resonance peaks because it contains several different diffraction order modes [29], [30]. However, it is difficult to fabricate ULPFG using resistive filament heating. The resonance peak appeared at the position of the maximum coupling coefficient only. The coupling coefficients of the tapered ULPFG were affected by weak modulation of the CO_2 laser. Then, a new resonance Peak B appeared compared to the original spectrum. Because Peak A and B were produced by the interactions between the fundamental core mode and different diffraction order modes, respectively, Peak B exhibited higher strain sensitivity.
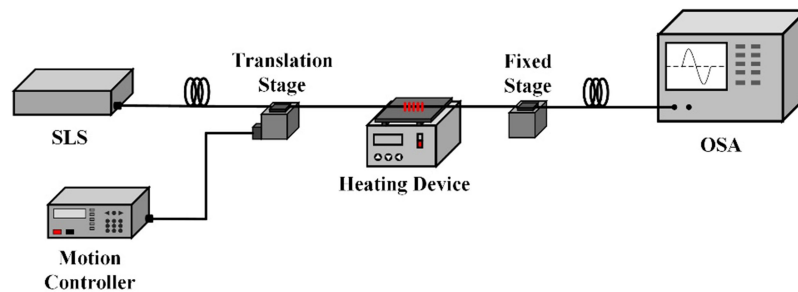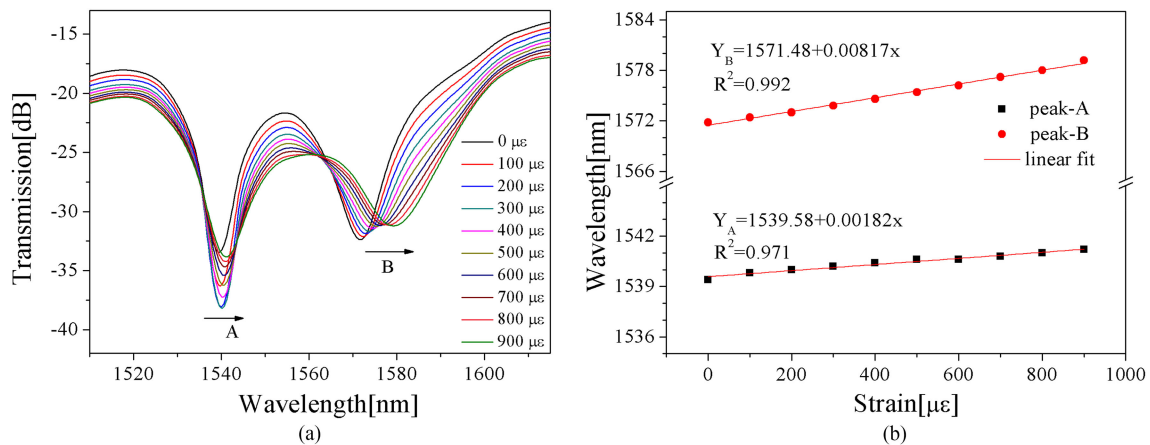
Fig. 5. Schematic of measurement set-up.

Fig. 6. Strain sensitivity of the sensor. (a) Transmission spectra. (b) Resonant wavelength shift of Peaks A and B.

3. Experimental Results and Discussions

Fig. 5 presents a diagram of the strain and temperature measurement set-up. The fiber ends were fixed on the two translation stages, which were used to pull the fiber and add strain to the grating. The fiber was connected with an SLS on one side and an OSA on the other to monitor spectrum change as the strain changed.

The transmission spectrum of grating changes in response to the applied strain is shown in Fig. 6(a). The resonance wavelengths demonstrated a red shift as the strain increased. The resonant wavelength of Peak A shifted from 1539.4 nm to 1541.2 nm, and Peak B shifted from 1571.8 nm to 1579.2 nm when the strain increased from 0 $\mu\varepsilon$ to 900 $\mu\varepsilon$. As depicted in Fig. 6(b), the wavelengths of Peaks A and B changed with increasing strain. The strain sensitivities of Peaks A and B were 1.82 pm/$\mu\varepsilon$ and 8.17 pm/$\mu\varepsilon$, respectively. As we know, for the two peaks that are produced by splitting, they come from the similar mode and the performance parameters of the two peaks don't differ greatly. However, the properties of Peaks A and B were quite different. Therefore, the peak B is a new peak really rather than a peak splitting.

As presented in Fig. 7(a), the modulated tapered LPFG was tested based on temperature. The resonance wavelengths exhibited a red shift as the temperature rose from 30 °C to 90 °C; Peak A shifted from 1540.3 nm to 1543.2 nm, and Peak B shifted from 1571.4 nm to 1575.3 nm. As depicted in Fig. 7(b), the temperature sensitivity of Peak A was 47.9 pm/°C, and that of Peak B was 65 pm/°C.

The aforementioned strain and temperature experiment demonstrated that strain and temperature could be measured simultaneously by detecting the resonant wavelength of Peaks A and B. The
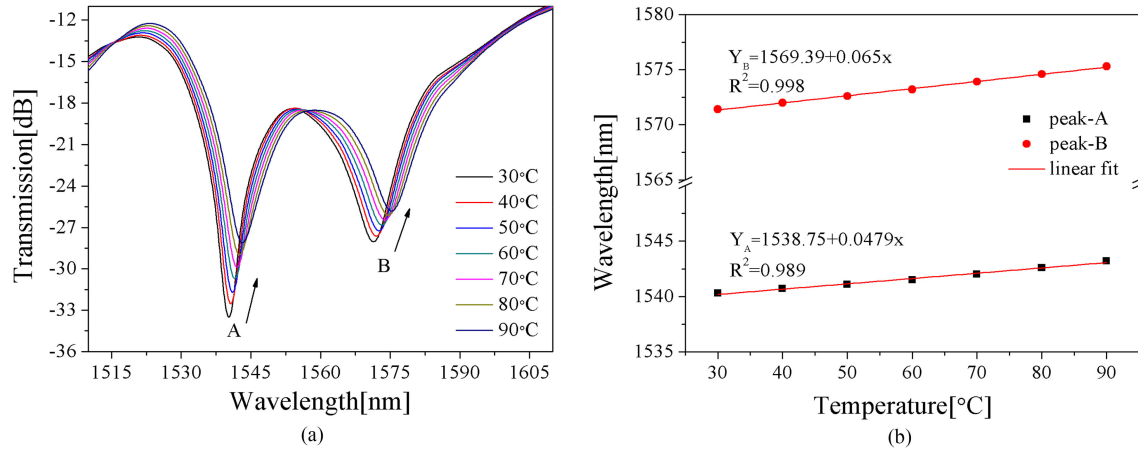
Fig. 7. Temperature sensitivity of the sensor. (a) Transmission spectra. (b) Resonant wavelength shift of P eaks A and B.
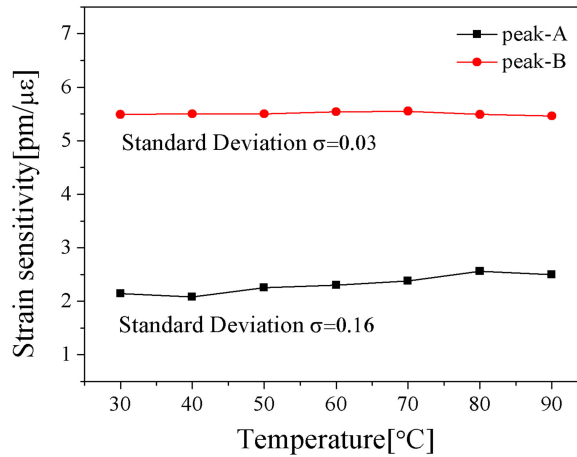

Fig. 8. Strain sensitivities of two peaks at different temperatures.

influence of temperature and strain on the grating can be expressed in matrix form as

$$\begin{pmatrix}\Delta T \\ \Delta \varepsilon\end{pmatrix} = \frac{1}{D}\begin{pmatrix} K_{\varepsilon \Delta \lambda_B} & -K_{\varepsilon \Delta \lambda_A} \\ -K_{T \Delta \lambda_B} & K_{T \Delta \lambda_A}\end{pmatrix}\begin{pmatrix}\Delta \lambda_A \\ \Delta \lambda_B\end{pmatrix} \tag{5}$$

where $D = K_{\varepsilon \Delta \lambda_B} K_{T \Delta \lambda_A} - K_{\varepsilon \Delta \lambda_A} K_{T \Delta \lambda_B}$. $\Delta \lambda_A$ and $\Delta \lambda_B$ represent the wavelengths shift of the two peaks; ΔT and $\Delta \varepsilon$ denote the respective temperature and strain variations; and $K_{\varepsilon \Delta \lambda_A}$, $K_{\varepsilon \Delta \lambda_B}$, and $K_{T \Delta \lambda_A}$, $K_{T \Delta \lambda_B}$ are the strain sensitivities and temperature sensitivities of Peaks A and B, respectively. From the aforementioned experimental results, $K_{\varepsilon \Delta \lambda_A} = 1.82$ pm/$\mu \varepsilon$, $K_{\varepsilon \Delta \lambda_B} = 8.17$ pm/$\mu \varepsilon$ and $K_{T \Delta \lambda_A} = 47.9$ pm/$^\circ$C, $K_{T \Delta \lambda_B} = 65$ pm/$^\circ$C. According to Matrix (1), the temperature and strain measurement can be given by

$$\begin{pmatrix}\Delta T \\ \Delta \varepsilon\end{pmatrix} = \frac{1}{273}\begin{pmatrix}8.17 & -1.82 \\ -65 & 47.9\end{pmatrix}\begin{pmatrix}\Delta \lambda_A \\ \Delta \lambda_B\end{pmatrix} \tag{6}$$

According to Matrix (6), variations in temperature and strain can be calculated by measuring the wavelength shifts of Peaks A and B. In our experiment, the wavelength resolution of the OSA is 0.02 nm, the calculated strain resolution was 1.25 $\mu \varepsilon$ and the calculated temperature resolution was 0.47 $^\circ$C. The measurement stability of the structure was confirmed as indicated in Fig. 8.

TABLE 1

Comparison of the Performance of the Reported Fiber Sensors for Simultaneous Strain and Temperature Measurement

references	Sensor structure	Fiber type	strain sensitivities	temperature sensitivities
[15]	cascade long period fiber grating (LPFG)	SMF	-0.95 pm/με, 0 pm/με	80 pm/°C , 69 pm/°C
[16]	cascade fiber Bragg grating	SMF, MMF	0.48 pm/με, -0.45 pm/με	9 pm/°C, 52 pm/°C
[17]	a fiber grating inscribed on a special optical fiber	High-Birefringent Fiber	1.08 pm/με, -1.36 pm/με	-37.84 pm/°C, 101.08 pm/°C
[19]	a LPFG induced by electric-arc discharge	SMF	-0.6 pm/με, -0.52 pm/με	30.9pm/°C, 68.1 pm/°C
[20]	a LPFG cascading another fiber structure	SMF, three-core fiber	-3 pm/με, -1.5 pm/με	43 pm/°C, 47 pm/°C
[22]	micro-tapered fiber grating	SMF	-0.55 pm/με	49.6 pm/°C
[23]	asymmetrical fiber Mach-Zehnder interferometer	SMF	-1.51 pm/με, -2.76 pm/με	60.1 pm/°C, 63.3 pm/°C
[24]	spheroidal-cavity-overlapped FBG	SMF	1.4 pm/με, 3.76 pm/με	8.4 pm/°C, 0.67 pm/°C
this study	secondary modulated tapered LPFG	SMF	1.82 pm/με, 8.17 pm/με	47.6 pm/°C, 65 pm/°C

The comparison between the fiber senor for simultaneous strain and temperature measurement in our study and other previously reported fiber sensors was listed in Table 1. It indicated advantages of the sensor structure proposed in this study including low cost using the standard single-mode fiber, easy fabrication, high strain sensitivity and the possibility of double parameters measurement.

4. Conclusion

In summary, a novel structure is proposed and tested to realize simultaneous measurement of strain and temperature. It was fabricated by weak power modulation of CO_2 laser exposure on the tapered LPFG. Because of the refractive index changed caused by weak power modulation, a new peak appeared. The two peaks have a red shift with the increasing strain and temperature. Experimental results revealed the strain and temperature sensitivities of the two peaks to be 1.82 pm/$\mu\varepsilon$, 47.9 pm/°C and 8.17 pm/$\mu\varepsilon$, 65 pm/°C, respectively. The respective strain and temperature resolution were 1.25 $\mu\varepsilon$ and 0.47 °C. This structure has the advantages of low cost, high strain sensitivity and good measurement stability. Thus, the sensor has great potential for applications in many fields.

References

[1] V. Bhatia and A. M. Vengsarkar, "Optical fiber long-period grating sensors," *Opt. Lett.*, vol. 21, no. 9, pp. 692–694, May. 1996.
[2] K. T. V. Grattan and T. Sun, "Fiber optic sensor technology: An overview," *Sens. Actuators A Phys.*, vol. 82, no. 1, pp. 40–61, 2000.

[3] E. Chehura, S. W. James, and R. P. Tatam, "Temperature and strain discrimination using a single tilted fiber Bragg grating," *Opt. Commun.*, vol. 275, pp. 344–347, 2007.

[4] L. Wang *et al.*, "Simultaneous strain and temperature measurement by cascading few-mode fiber and single-mode fiber long-period fiber gratings," *Appl. Opt.*, vol. 53, no. 30, pp. 7045–7049, Oct. 2014.

[5] Z. Y. Bai *et al.*, "Simultaneous measurement of strain and temperature using a long period fiber grating based on waist-enlarged fusion bitapers," *J. Opt.*, vol. 16, 2014, Art. no. 045401.

[6] M. Xiong, H. Gong, Z. Wang, C.-L. Zhao, and X. Dong, "Simultaneous refractive index and temperature measurement based on mach-zehnder interferometer concatenating two Bi-tapers and a long-period grating," *IEEE Sensors J.*, vol. 16, no. 11, pp. 4295–4299, Jan. 2016.

[7] K. Naeem, B. H. Kim, B. Kim, and Y. Chung, "Simultaneous multi-parameter measurement using Sagnac loop hybrid interferometer based on a highly birefringent photonic crystal fiber with two asymmetric cores," *Opt. Exp.*, vol. 23, no. 3, pp. 3589–3601, Feb. 2015.

[8] A. Layeghi and H. Latifi, "Tunable ferrofluid magnetic fiber sensor based on nonadibatic tapered Hi-Bi fiber in fiber loop mirror," *J. Lightw. Technol.*, vol. 36, no. 4, pp. 1097–1104, Feb. 2018.

[9] H. Ying, B. K. Chen, G. D. Chen, H. Xiao, and S. U Khan, "Simultaneous detection of liquid level and refractive index with a long-period fiber grating based sensor device," *Meas. Sci. Technol.*, vol. 24, no. 9, 2013, Art. no. 095303.

[10] S. Y. Zhao, J. W. Cui, C. Q. Yang, Z. Y. Ding, and J. B. Tan, "Simultaneous measurement of shape and temperature in the substrate-attaching-fibers sensing system," *IEEE Photo. J.*, vol. 9, no. 6, Dec. 2017, Art. no. 6805009.

[11] K. Bremer, T. Reinsch, G. Leen, B. Roth, S. Lcohmann, and E. Lewis, "Pressure, temperature and refractive index determination of fluids using a single fibre optic point sensor," *Sens. Actuators A Phys.*, vol. 256, pp. 84–88, 2017.

[12] Y. M. Raji, H. S. Lin, S. A. Ibrahim, M. R. Mokhtar, and Z. Yusoff, "Intensity-modulated abrupt tapered fiber Mach-Zehnder Interferometer for the simultaneous sensing of temperature and curvature," *Optics Laser Technol.*, vol. 86, pp. 8–13, 2016.

[13] K. L. Ren *et al.*, "Highly strain and bending sensitive microtapered long-period fiber gratings," *IEEE Photon. Technol. Lett.*, vol. 29, no. 13, pp. 1085–1088, Jul. 2017.

[14] Y. L. Zheng, K. Bremer, and B. Roth, "Investigating the strain, temperature and humidity sensitivity of a multimode graded-index perfluorinated polymer optical fiber with Bragg grating," *Sensors.*, vol. 18, no. 5, p. 1436, May. 2018.

[15] H. Y. Zeng *et al.*, "Combining two types of gratings for simultaneous strain and temperature measurement," *IEEE Photon. Technol. Lett.*, vol. 28, no. 4, pp. 477–480, Feb. 2016.

[16] H. Sun, "Simultaneous measurement of temperature and strain or temperature and curvature based on an optical fiber Mach-Zehnder interferometer," *Opt. Commun.*, vol. 340, pp. 39–43, 2015.

[17] Y. W. Lee *et al.*, "Polarization-insensitive discrimination of strain and temperature based on long-period fiber grating inscribed on high-birefringent fiber ended with Faraday rotator mirror," *Jpn. J. Appl. Phys.*, vol. 45, 2006.

[18] K. J. Han, Y. W. Lee, J. Kwon, S. Roh, J. Jung, and B. Lee, "Simultaneous measurement of strain and temperature incorporating a long-period fiber grating inscribed on a polarization-maintaining fiber," *IEEE Photon. Technol. Lett.*, vol. 16, no. 9, pp. 2114–2116, Sept. 2004.

[19] C. Du, Q. Wang, and Y. Zhao, "Long-period fiber grating sensor induced by electric-arc discharge for dual-parameter measurement," *Instrum. Sci. Technol.*, vol. 46, no. 1, pp. 1–11, 2018.

[20] T. Geng *et al.*, "Modal interferometer using three-core fiber for simultaneous measurement strain and temperature," *IEEE Photo. J.*, vol. 8, no. 4, Aug. 2016. Art. no. 6803908.

[21] Y. J. Rao, Z. L. Ran, X. Liao, and H. Y. Deng, "Hybrid LPFG/MEFPI sensor for simultaneous measurement of high-temperature and strain," *Opt. Exp.*, vol. 15, no. 22, pp. 14936–14941, Oct. 2007.

[22] M. S. Yoon, S. Park, and Y. G. Han, "Simultaneous measurement of strain and temperature by using a micro-tapered fiber grating," *J. Lightw. Technol.*, vol. 30, no. 8, pp. 1156–1160, Apr. 2012.

[23] P. Lu and Q. Y. Chen, "Asymmetrical fiber Mach-Zehnder interferometer for simultaneous measurement of axial strain and temperature," *IEEE Photo. J.*, vol. 2, no. 6, pp. 942–953, Dec. 2010.

[24] Y. Pan *et al.*, "Simultaneous measurement of temperature and strain using spheroidal-cavity-overlapped FBG," *IEEE Photo. J.*, vol. 7, no. 6, Dec. 2015. Art. no. 6803406.

[25] R. Xing *et al.*, "Simultaneous strain and temperature sensor based on polarization maintaining fiber and multimode fiber," *Opt. Laser Technol.*, vol. 102, pp. 17–21, 2018.

[26] W. L. Yang *et al.*, "A phase-shifted long period fiber grating based on filament heating method for simultaneous measurement of strain and temperature," *J. Opt.*, vol. 17, no. 7, 2015.

[27] L. Jin, W. Jin, J. Ju, and Y. Wang, "Coupled local-mode theory for strongly modulated long period gratings," *J. Lightw. Technol.*, vol. 28, no. 12, pp. 1745–1751, Jun. 2010.

[28] L. Jin, W. Jin, J. Ju, and Y. P. Wang, "Investigation of long-period grating resonances in hollow-core photonic bandgap fibers," *J. Lightw. Technol.*, vol. 29, no. 11, pp. 1708–1714, Jun. 2011.

[29] T. Zhu, Y. J. Rao, and J. L. Wang, "Characteristics of novel ultra-long-period fiber gratings fabricated by high-frequency CO_2 laser pulses," *Opt. Commun.*, vol. 277, pp. 84–88, 2007.

[30] Y. J. Rao, T. Zhu, and Q. J. Mo, "Highly sensitive fiber-optic torsion sensor based on an ultra-long-period fiber grating," *Opt. Commun.*, vol. 266, pp. 187–190, 2006.